Artificial Neural Network (ANN) modeling of the pulsed heat load during ITER CS magnet operation

# Artificial Neural Network (ANN) Modeling of the Pulsed Heat Load during ITER CS Magnet Operation

L. Savoldi Richard[a], R. Bonifetto[a], S. Carli[a], A. Froio[a], A. Foussat[b] and R. Zanino[a]

[a] *Dipartimento Energia, Politecnico di Torino, Corso Duca degli Abruzzi 24, 10129 Torino,Italy*
[b] *ITER International Organization, St.Paul-lez-Durance, France*

## Abstract

Artificial Neural Networks (ANNs) are applied to the development of a simplified transient model of the ITER Central Solenoid (CS), aiming at predicting the evolution of the pulsed heat load from the CS to the LHe bath during plasma operation. The ANNs are trained using the thermal-hydraulic evolution in the CS, computed with the 4C code, due to AC losses,. The capability of the ANN model to predict the heat load to the LHe bath is successfully demonstrated in the case of different transients, among which a nominal plasma operating scenario. The gain in speed of the simplified model with respect to the 4C code results is by order of magnitudes, with a small loss of accuracy.

**Keywords:** artificial neural networks; nuclear fusion; ITER; superconducting magnets; central solenoid; pulsed heat load

**Abbreviations and symbols**

| ***Nomenclature*** | |
|---|---|
| ANN – Artificial Neural Network | OD – outer diameter |
| BV – bypass valve | $p$ – He pressure |
| AC – alternating current | $P$ – Power |
| C# – connection pipe # | $Q$ – thermal power |
| CICC – cable-in-conduit conductor | QP – quad-pancake |
| CPU – Central Processing Unit | RRR – residual resistivity ratio |
| CS – Central Solenoid | SC – superconducting |
| CV – control valve | SHe – supercritical Helium |
| $dm/dt$ – mass flow rate | SOD – start of discharge |
| E – energy | $T$ – He temperature (K) |
| EOB – end of burn | $t$ – time |
| $h$ – specific He enthalpy | V# – manifold/volume # |
| HELIOS – HElium Loop for hIgh LOads Smoothing | 4C – Cryogenic Circuit Conductor and Coil code |
| HX – Heat eXchanger | Greek |
| HP – hexa-pancake | $\Delta$ – difference |
| i – index | $\varepsilon$ – relative error |
| ID – inner diameter | $\Sigma$ – sum |
| IM – initial magnetization | Subscripts |
| ITER – International Thermonuclear Experimental Reactor | in – inlet |
| LHe – Liquid Helium | NN – neural network |
| | 0 – initial |

## 1. INTRODUCTION

The assessment of the operation of the cryoplants in large fusion machines with superconducting (SC) coils, such as ITER, is becoming of increasing relevance, in view of the cost of the SC magnet [1] operation. The smoothing of the pulsed load to the refrigerator is carefully under consideration to limit an expensive over-sizing of the refrigerators [2]. On this track, different strategies are being developed both through experiments, e.g. in the HELIOS facility [3-4] at CEA Grenoble, France, and through dedicated analysis [5-9], performed with different computational tools.

The 4C code [10], developed for and dedicated to the detailed simulation of the magnet thermal-hydraulic transients during, for instance, plasma operating scenarios [11-12], can be adopted to test the measure of success of different control strategies. However, the assessment of the cryoplant operation does not require many details from the magnet side, which can be easily computed by 4C, but mainly the evolution of the heat load to the liquid helium (LHe) baths that are used as interfaces/buffers between the magnets cooling loops and the cryoplant. While simplified physics-based models to address this issue are under development [13], a different innovative approach

for a simplified dynamic model of the pulsed heat load from the superconducting magnets to the LHe baths has been recently presented [14] based on Artificial Neural Networks (ANNs) [15], and its capability to properly reproduce the dynamic evolution of a supercritical helium (SHe) loop has been shown against HELIOS dynamics. For the heated pipes that mimic in HELIOS the superconducting magnets, the ANN builds a mathematical input/output relation, just relying on the "rules" learned based on a small set of "training" cases, obtained from the simulations using the comprehensive 4C code. Although a burdensome training phase is needed when using ANNs and no physical content is stored in the network, a great advantage of this approach with respect to the extensive use of the 4C code, where the physics content is very high, is the speed of execution, with a small loss of accuracy.

Here we apply for the first time this novel approach to a full-scale superconducting magnet system, and namely the ITER Central Solenoid. The paper is organized as follows: we first introduce the 4C model of the ITER CS, then we show how the complex CS modeling can be split in simpler problems, each involving only a CS module. For each module, we develop and train a suitable ANN, that we then apply to predict the heat load evolution at the bath during an ITER standard operating scenarios. The ANN prediction is compared with the result computed by 4C, both in terms of accuracy and in terms of computational effort (time) needed to get the results.

## 2. 4C MODEL OF THE ITER CS COIL

The ITER CS magnet is constituted by 6 different modules, cooled by Supercritical Helium (SHe) in forced flow in a hydraulic parallel and releasing the heat load to a LHe bath through a heat exchanger located downstream of the circulator, see Fig. 1. The three upper modules (CSU) are first connected in a tight parallel through suitable piping and manifolds, and only at a second level connected to the tight parallel between the CS lower (CSL) modules, see Fig. 1. For the time being, the LHe bath will be considered as the interface with the refrigeration system, and it will be assumed to be at the constant temperature of 4.3 K.

Each CS module is constituted by six hexa-pancakes (HP) and a single quad-pancake (QP), connected through electrical joints located on the outer side of the module, see Fig. 2a. The HPs and the QP are wound using a circle-in-square Nb3Sn Cable-in-Conduit Conductor, see Fig. 2c, whose main features are summarized in Table 1. Since each pancake is separately fed by a helium inlet located on the inner side of the module, it represents a single hydraulic channel: the 4C model accounts for the 40 separate hydraulic channels in each module, whose main features are summarized in Table 2. The thermal coupling inside each module, i.e. the inter-turn/inter-pancake is accounted for in the 4C code by means of local thermal bridges connecting at any point each hydraulic channel with the neighboring ones. The thermal resistance between adjacent turns and layers is simply computed as a series of thermal resistances due to the multi-layer insulation, see Fig. 2b.

In the 4C model of the whole ITER CS, all 6 modules are considered simultaneously, with a total of $6 \times 40 = 240$ hydraulic channels connected to the cryogenic circuit as shown in Fig. 1. The operating point computed for the circuit corresponds to a pump pressure head of ~ 0.115 MPa, with a mass flow rate of ~1.53 kg/s (~6.38 g/s in each

hydraulic channel, conservatively slightly lower than the nominal value foreseen during ITER operation). This model will be indicated as Model 1 in what follows. The main parameters used in Model 1 are reported in Table 3.

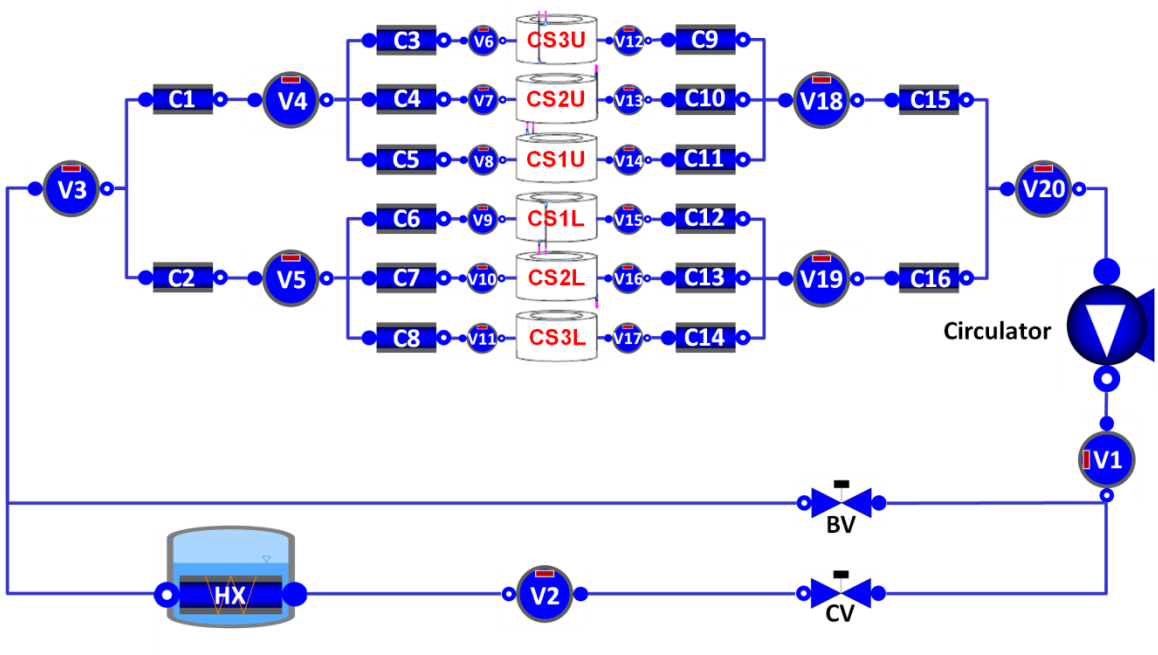


**Fig. 1 – Model 1: 4C model of the ITER CS coil cooling circuit.**

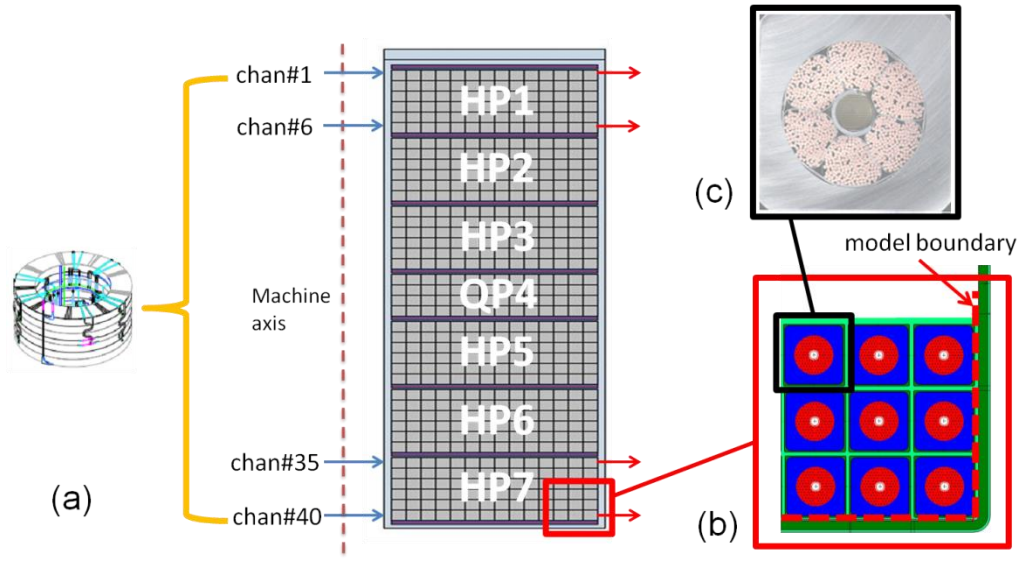


**Fig. 2 – Cross section of an ITER CS module (a), with a zoom showing the insulation layer between adjacent turns (b) down to a single CICC (c).**

**Table 1 – Main parameters of the ITER CS conductor.**

| Item | Value |
|---|---|
| SC strands number | 576 |
| Strands diameter | 0.83 mm |
| $Nb_3Sn$ strand Cu-to-non-Cu ratio | 1.0 |
| Non copper area | 154.3 $mm^2$ |
| Total copper area | 308.6 $mm^2$ |
| Cos(θ) | 0.96 |
| Cu RRR | 100 |

**Table 2 – Main parameters of each hydraulic channel in any CS coil module.**

| Item | Value |
|---|---|
| Conductor length in 1 module | 6019 m |
| Hydraulic channel length | 150.48 m |
| Number of turns | 14 |
| Turn length | 10.75 m |
| Cable diameter | 32.6 mm |
| Jacket external side | 49 mm |
| He cross section in the annulus | 258.77 $mm^2$ |
| Void fraction in the annulus | 33.5% |
| Wetted perimeter of the annulus (twisted strands) | 2.56 m |
| Central channel ID/OD | 7 mm / 9 mm |
| Surface perforation from central channel to bundle | 10% |
| Friction factor correlation (bundle) | $(0.0231+19.5/(Re)^{0.7953})/ (voidFraction^{0.742})$ |
| Friction factor correlation (central channel) | $0.45\times(Re)^{-0.034}$ |

**Table 3 – Main parameters of the cryogenic circuit components of Model 1.**

| Component | Name | Characteristic | | | |
|---|---|---|---|---|---|
| | | length (m) | diameter (mm) | | |
| Pipes | C1, C15 | 40 | 85 | | |
| | C2, C16 | 96 | 85 | | |
| | C3-C14 | 54 | 53 | | |
| | | area ($mm^2$) | opening (%) | | |
| Valves | CV | 707 | 100 | | |
| | BV | 707 | 0 | | |
| | | volume ($m^3$) | | | |
| Manifolds | V1-V3, V20 | 0.24 | | | |
| | V4, V5, V18, V19 | 0.164 | | | |
| | V6-V17 | 0.4 | | | |
| | | length (m) | diameter of pipes (mm) | # of parallel pipes | $T_{bath}$ (K) |
| Heat eXchangers | HX1 | 31 | 20 | 64 | 4.3 |

Since the CS coil is subject to pulsed operation, its main thermal-hydraulic driver is represented by the AC losses in the conductors, which are deposited according to a given spatial distribution, that changes in time along each hydraulic channel, as reported in normalized form in Fig. 3, for instance for channel #4 in CS1U during a standard 15 MA inductive plasma operation, whose sequence of events is reported in Fig. 4 [17].

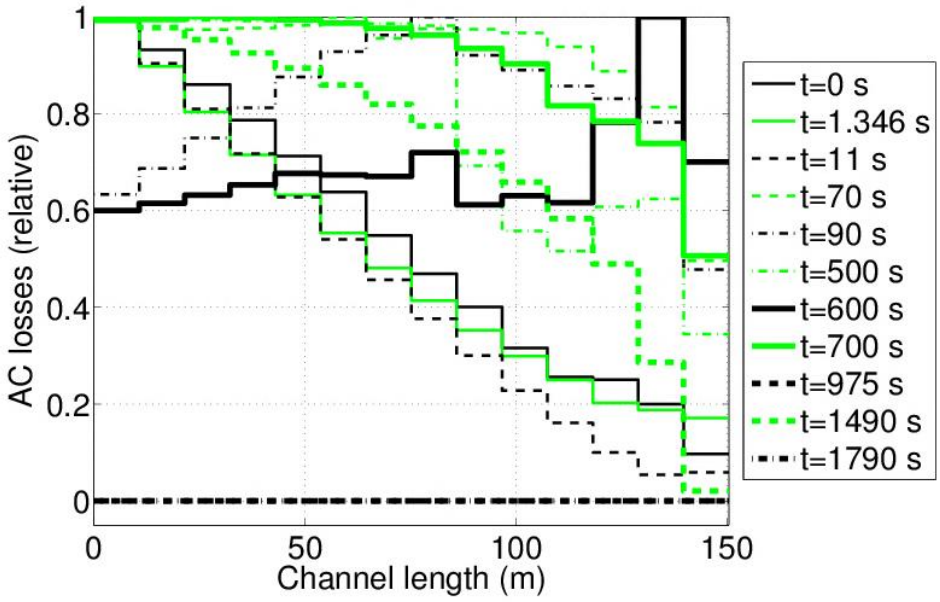


**Fig. 3 – Map of the normalized heat load by AC losses deposited during a standard 15 MA plasma operating scenario in the hydraulic channel #4 of the CS1U module [17].**

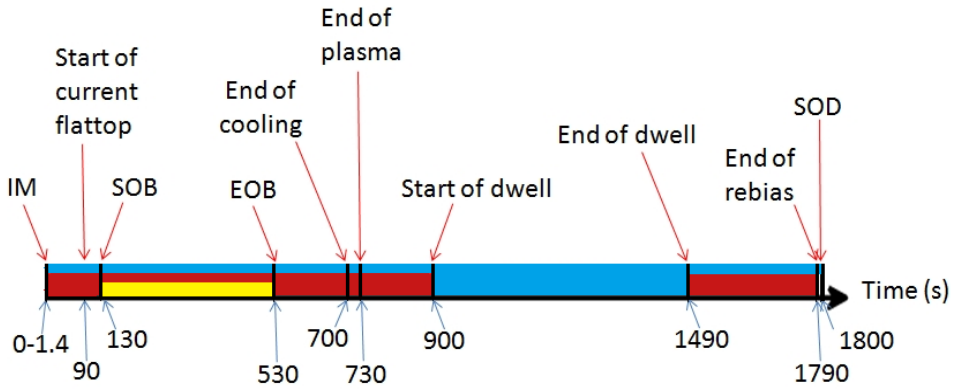


**Fig. 4 – Time line of the standard 15 MA scenario foreseen in ITER (IM = initial magnetization, SOB = start of burn, EOB = end of burn, SOD = start of discharge). The radiative (static) load on the cryolines is present during the whole 1800 s (blue line) and the AC losses according to the red line.**

In [14], the driver of the thermal-hydraulic transients inside the loop was the heat deposition in (three) different pipes (no superconducting cables are present in HELIOS), but there the heated entities (= pipes) were connected hydraulically in series, while the different CS modules and the pancakes in each module, corresponding here to the heated entities, are connected in parallel (see Fig. 1 and Fig. 2, respectively). The different connection implies that in the 4C model of HELIOS the evolution of pressure $p$ and temperature $T$ at the HX inlet could hardly be obtained merely there as the sum of $T$ and $p$ increase due to the separate operation of each single heated pipe because of the non-linear effect of the mass flow rate, forced to pass through all the heated pipes in series, so that the sum (superposition) of the effects was only pursued for the heat flux released to the LHe bath. On the contrary, in the ITER CS also the evolution of pressure and temperature at the HX inlet can be likely obtained by "superposition of the effects" of the separate thermal-hydraulic evolution induced by each module due to the hydraulic parallel connection of the modules. Each module can be analyzed separately from the others, and the global thermal hydraulic evolution at the HX when the full coil is considered can be just obtained by the sum of the variation of $p$ and $T$ due to all single modules. At this stage, to further simplify the problem, the simulation of a thermal-hydraulic transient in any single module can be reasonably done on a rescaled cryogenic circuit model (Model 2, see Fig. 5), where all the pipe cross sections and manifold volumes have been divided by the number of modules as reported in Table 4, preserving the transit time in the circuit, and the pump characteristic has been also rescaled to 1/6 of the original nominal mass flow, keeping the same pressure head.

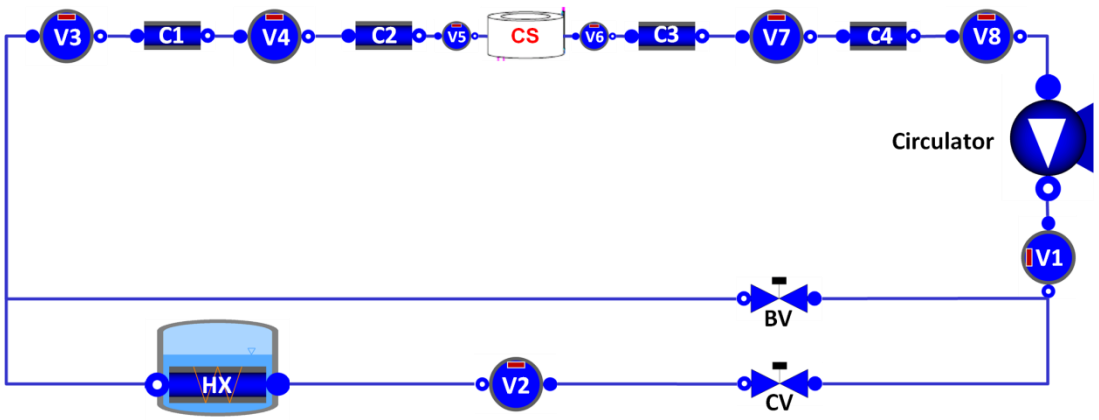


**Fig. 5 – Model 2: 4C model of the cooling circuit of each ITER CS module.**

**Table 4 – Main parameters of the cryogenic circuit components of Model 2.**

| Component | Name | Characteristic | | | |
|---|---|---|---|---|---|
| | | length (m) | diameter | | |
| Pipes | C1, C4 | 40 (U), 96 (L) | 49.07 | | |
| | C2, C3 | 54 | 53 | | |
| | | area ($mm^2$) | opening (%) | | |
| Valves | CV | 117.83 | 100 | | |
| | BV | 117.83 | 0 | | |
| | | volume ($m^3$) | | | |
| Manifolds | V1-V3, V8 | 0.04 | | | |
| | V5, V6 | 0.4 | | | |
| | V4, V7 | 0.05467 | | | |
| | | length (m) | diameter of pipes (mm) | # of parallel pipes | $T_{bath}$ (K) |
| Heat eXchangers | HX | 31 | 8 | 64 | 4.3 |

The validation of this simplifying approach is reported in Fig. 6. The same heat load per module, having the waveform reported in Fig. 6a, is applied first in Model 1, and then separately in the Model 2 of each of the six CS modules. In each channel, for each module, the spatial power distribution peculiar of the first phase of the standard 15 MA plasma scenario (between 11 and 70 s from the IM, when the largest fraction of the total energy is deposited, see below), see Fig. 4, is adopted. The evolution of pressure $p$, temperature $T$ at the HX inlet are then evaluated for the different simulations, and those computed in Model 1 are compared to the average of those computed for each module with Model 2, as reported in Fig. 6b-c. Notwithstanding the small differences in the mass flow rates between CSU and CSL coils, which are neglected here, the agreement in the results computed in the simulation of the whole CS coil with those obtained by the superposition of effects is excellent on all the thermal-hydraulic variables. Also the evolution of the power and cumulative energy released to the LHe bath (see Fig. 6c) show an excellent agreement that fully justifies the simplification of the CS model into six separate and independent sub-problems.

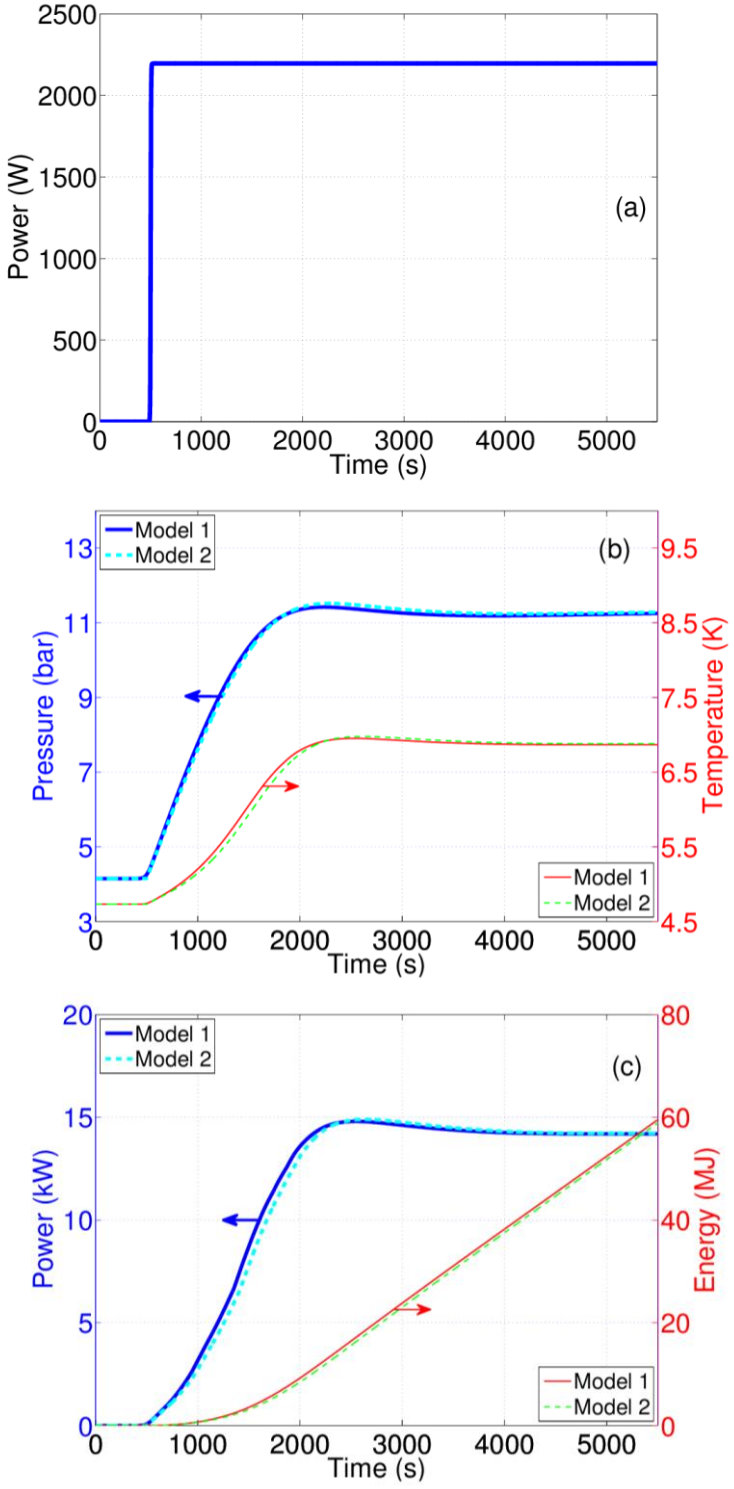


**Fig. 6 − Conceptual proof of the superposition of effects in the CS coil: (a) waveform of the power deposited in each of the CS modules. (b) Computed evolution pressure (left axis) and temperature (right axis) at the HX inlet and (c) evolution power (left axis) and energy (right axis) released to the LHe bath, computed in Model 1, or by the superposition of effects of Model 2.**

## 3. ANNs MODEL OF THE ITER CS COIL

Based on the proof of the superposition of the effects as given above, the development of the ANN for the CS coil can then be simplified into the development of an ANN for each of the CS module. The output of the different ANNs will be then used together to predict the evolution of thermal-hydraulic variables at the HX inlet as shown schematically in Fig. 7.

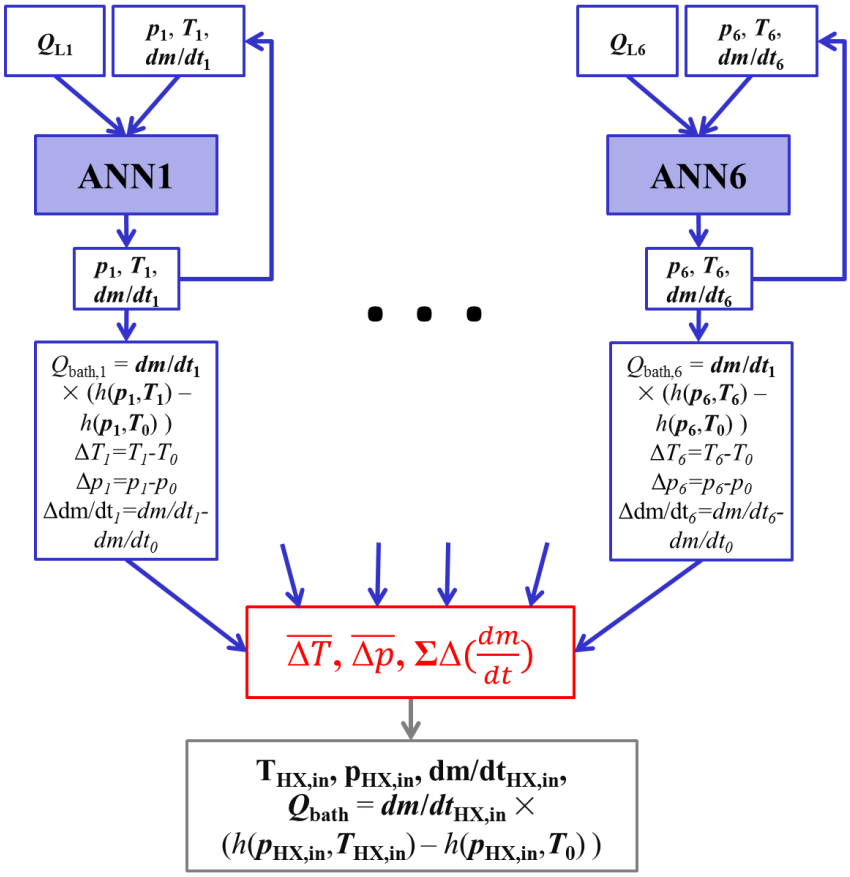


**Fig. 7 − The ANN structure adopted for the CS coil dynamic simulations.**

Since the ANN is just a sort of transfer function [15], it does not contain any physics information, but a proper choice of input and output variables, together with a well-educated training, can make it well reproduce and predict the dynamic evolution of a real (physical) system. The input variable chosen for the case at hand is the total power evolution in each CS module $Q_{Li}$, while the output variables represent the thermodynamic state of the system (pressure and temperature evolution, together with the evolution of the mass flow rate, all evaluated here at the HX inlet), see Fig. 7. Starting from the variables in output from each network, the power released to the LHe bath through the HX can be computed as:

$$Q_{bath} = -\left(\frac{dU}{dt}\right)_{HX} + \frac{dm(t)}{dt}\left[h(T(t),p(t)) - h(T_0,p(t))\right] \quad (1)$$

where $(dU/dt)_{HX}$ is the variation of internal energy of the Helium inside the HX, $h$ the specific enthalpy and $T_0$ the He temperature in the steady state before the heat deposition starts at the HX outlet - since the HX is close to ideal, this temperature is very close to that of the LHe bath. The internal energy variation in this case, assuming a temperature difference up to, say, 2-3 K in ~1000 s, remains below 200-300 W, which is only ~ 1% of the maximum power considered here, in view of the small volume of helium contained in the HX, see Table 4. We will then neglect this term in our balance.

Strongly relying on the kind of network already used in [14], we adopt here a dynamic network, with one input variable with two delays, hidden layers, and 3 outputs closed in feedback with one delay. (The specific recipe - 1 vs. 2 hidden layers, 6 vs. 10 neurons per layer - has been optimized on each single CS module.) A schematic view of the network inputs/outputs is reported in Fig. 8 in which the outputs at time $t-\Delta t$ (corresponding to one delay feedbacks) are fed, together with the input at times $t$ and $t-\Delta t$ (= two delays for the input variable). While the delays in the ANN help in properly following the transient behavior of the system, the feedback is here chosen to give back in input the infos about the thermodynamic state of the system [16].

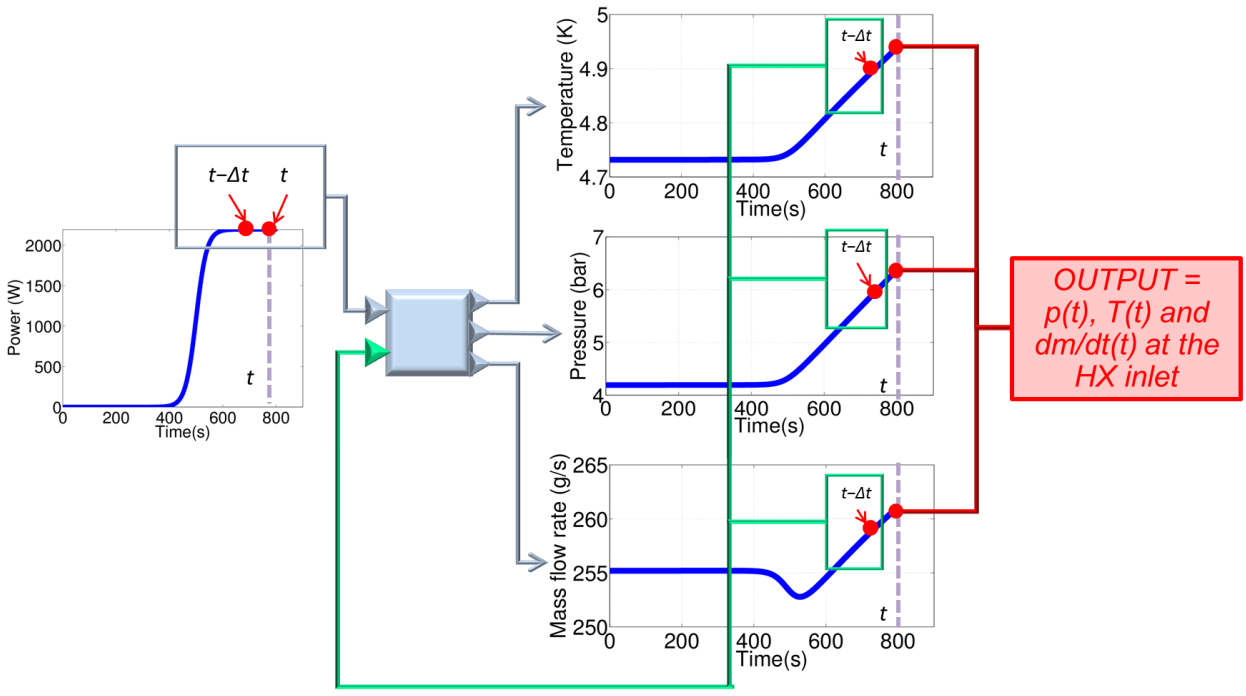


**Fig. 8 − Schematic view of the input/output variables selected for the ANN model of each CS module.**

## 3.1. Training of the ANNs of the different CS modules

The training of the different ANNs for each CS module has been performed using as training cases the 4C simulations based on Model 2 (see above), where the power in the different hydraulic channels has been applied as a sigmoid function (see [14]) with a total amplitude on the entire module scanning the range 200 W - 10000 W. Note

that this range does not cover the power peaks foreseen during a typical plasma operating scenario, see also below, but since we use it in training simulations were we follow the transient evolution up to steady state, higher power inputs would correspond to a circuit response completely out of the picture for ITER. The choice of the proper spatial distribution to be used in the training simulation is delicate, in view of the variation of the power distribution during the plasma operation transient, see Fig. 3. A spatial distribution much different from the one used in the training simulations would imply a change in the location of the energy input, and consequently a slightly different evolution of the thermodynamic variables at the HX, reducing the accuracy of the ANN predictions. This issue has been solved noting that, for most of the modules, the largest fraction of the total energy deposited during the standard 15 MA plasma scenario occurs between 11 and 70 s from the IM (Fig. 4), as reported in Fig. 9**Error! Reference source not found.** [17]. The spatial distribution corresponding to that phase has then been adopted for the training simulations.

During the training process, the input as well as the output variables are fed to the network, so that the weights and biases of the artificial neurons [14] can be identified through suitable training algorithms. The dedicated Matlab® Neural Network Toolbox [18] has been used for the network training.

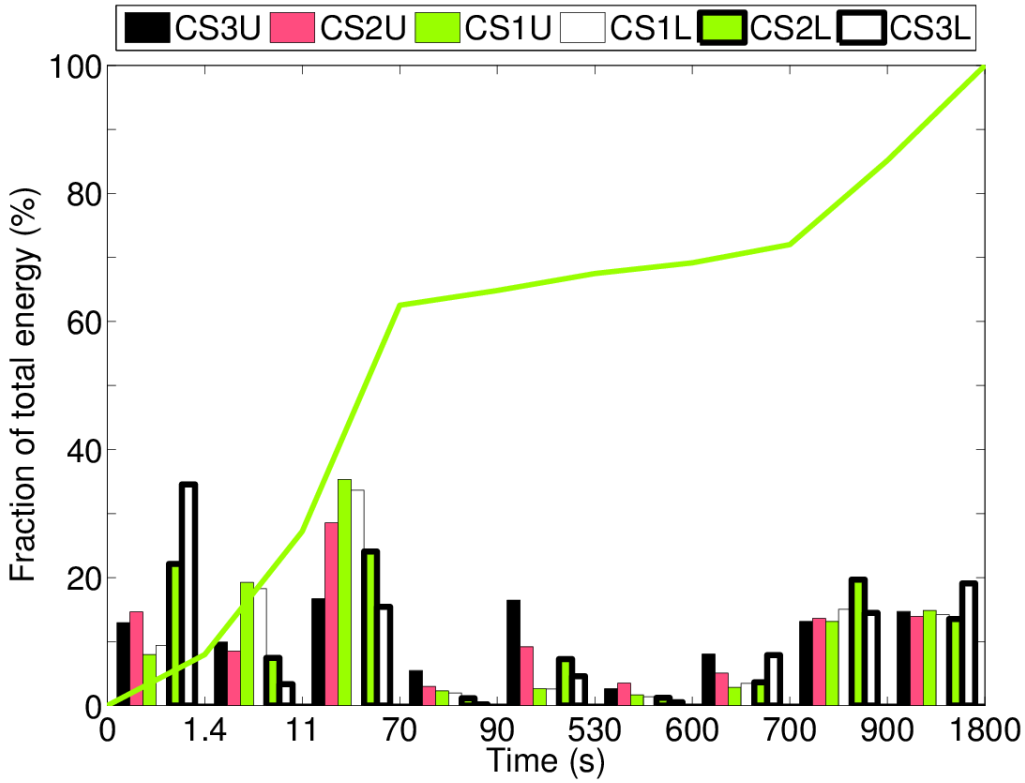


**Fig. 9 − Standard 15 MA plasma scenario. Histogram: fraction of the total energy deposited in each CS module during the different phases of the transient [17]. Solid line: evolution of the fraction of the total energy deposited in CS1U module during one period.**

## 4. PREDICTIVE CAPABILITIES OF THE ANN MODEL

Once the training process is concluded, the verification of the predictive capability of the ANN can be performed at different levels, for instance feeding each ANN with input waveforms never seen during the training process and checking the accuracy of the results and the corresponding gain in speed against the results provided by the 4C simulation performed using Model 2 and the same input power evolution. Than the prediction of the superposition of the 6 ANNs can be compared with the 4C results obtained using Model 1 above.

### 4.1. Sigmoid wave-form scenario for a single CS module

For the ANN corresponding to each CS module, the predictive capability has been first checked in a simple case where a power sigmoid waveform, reaching a power level never tested during the training process, is fed to the network. The comparison with the corresponding 4C results, in terms of $T(t)$, $p(t)$ and $dm(t)/dt$ at the HX inlet, is reported in Fig. 10 for the ANN developed for the module CS1U. The maximum relative error in the predictive variables is 4.6% on the pressure, while it remains below 2% for temperature and mass flow rate. The gain in the CPU time is ~ 25000 with respect to the 4C simulation.

The resulting prediction, in terms of evolution of the power and cumulative energy transferred to the LHe bath, is reported in Fig. 11a. The average relative error on the power, evaluated after the end of the sigmoid wave-form, is ~ 3.2% (Fig. 11b), while the relative error on the cumulative energy is ~ 0.15%, computed when the power release reaches the 99% of the steady-state value, see Fig. 11c. A similar picture is also found for the ANNs developed for the other modules, as reported in Fig. 11b-c. The small loss in accuracy is largely compensated by the gain in CPU time that for all modules is above $2\times10^4$.

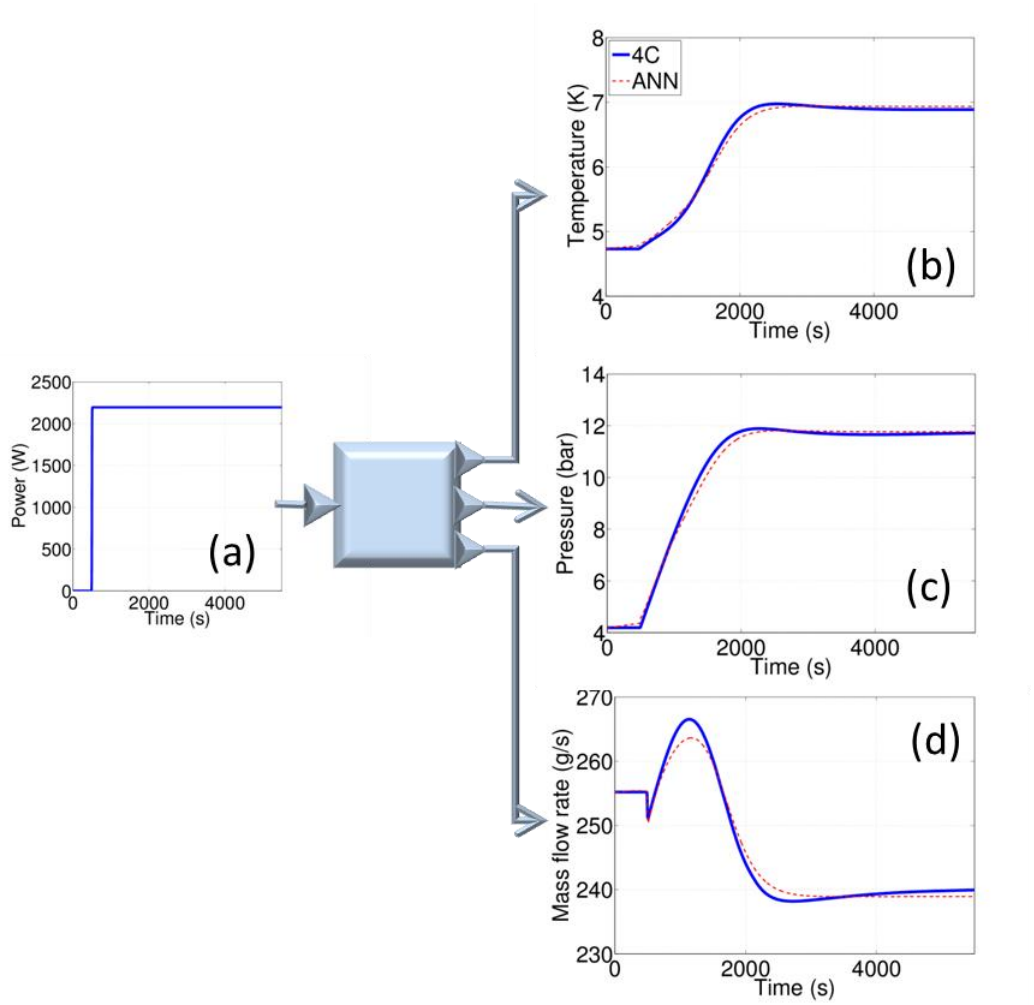


**Fig. 10 − Predictive test of ANN for the CS1U module: evolution of the sigmoid driver (a) and evolution of the predicted temperature, pressure and mass flow rate (dashed lines in (b), (c) and (d), respectively), compared to the respective signals computed by the 4C code (solid lines).**

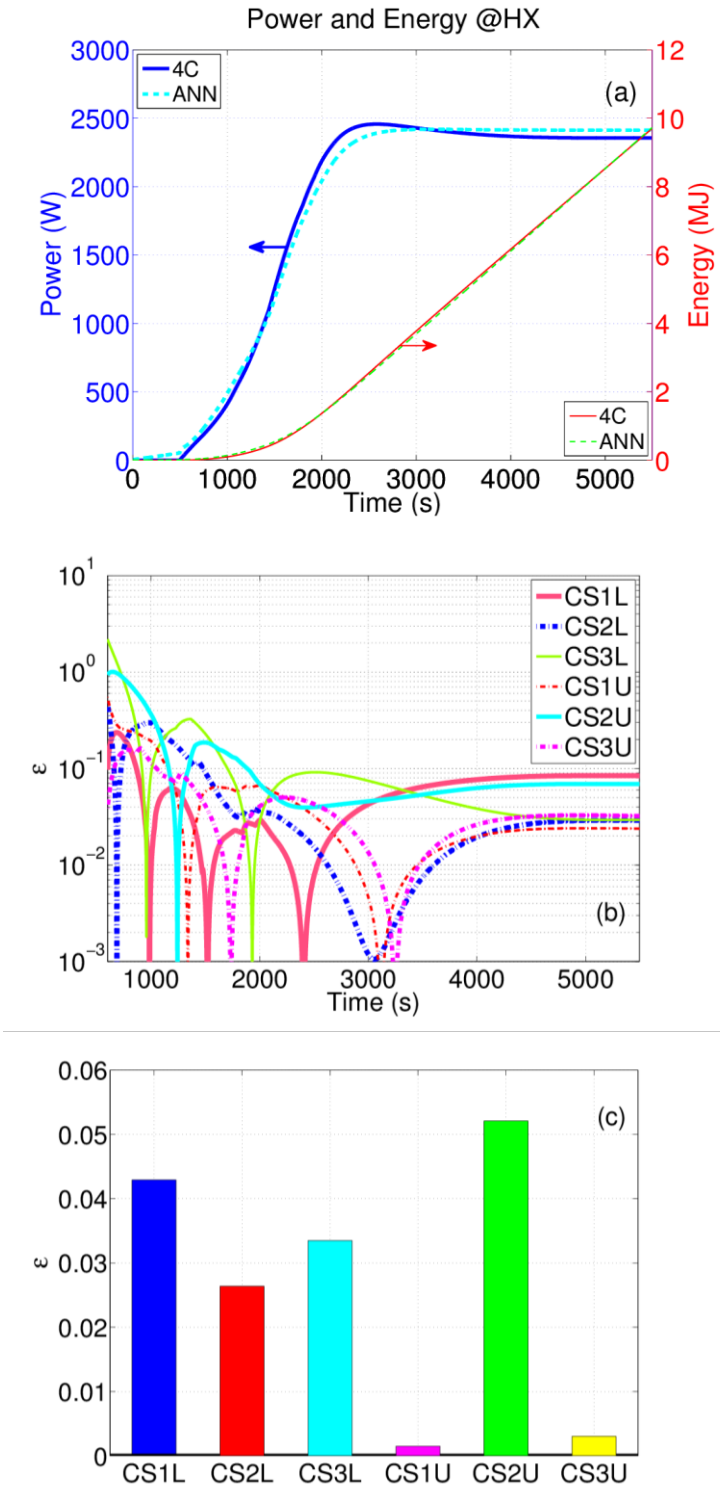


**Fig. 11 − Predictive tests of the ANNs of the different modules for sigmoid power waveform never seen during the training process: (a) evolution of the power (left axis, thick lines) and cumulative energy (right axis, thin lines) released to the HX predicted by the ANN (dashed lines) and computed by the 4C code (solid lines) for the CS1U; (b) evolution of the relative error on the power released to the HX; (c) relative error on the cumulative energy released to the HX (evaluated at the 99% of the power steady-state value).**

## 4.2. Plasma operation scenario for a single CS module

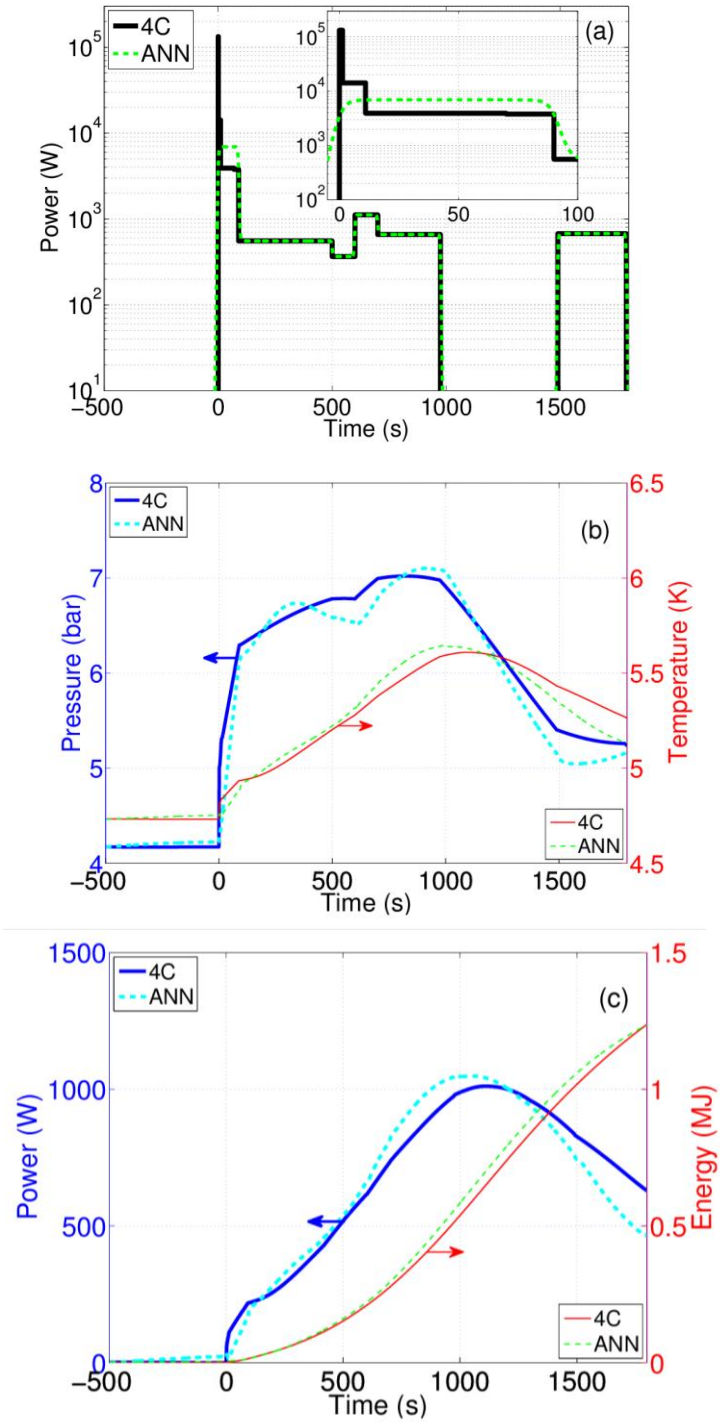


**Fig. 12 − Predictive test of ANN for the CS3U module: (a) power wave-form during one plasma pulse (solid), compared to the waveform as given in input to the ANN (dashed); (b) evolution of the pressure (left axis, thick lines) and temperature (right axis, thin lines) predicted by the ANN (dashed lines) compared to the results computed by 4C (solid lines); (c) evolution of the power (left axis, thick lines) and cumulative energy (right axis, thin lines) released to the HX predicted by the ANN (dashed lines) and computed by the 4C code (solid lines).**

Once the predictive capability of a network has been checked over a single sigmoid, any other power wave-form can be easily decomposed in a sequence of sigmoid functions, to be treated by superposition of effects. Each power step is approximated by a sigmoid having amplitude corresponding to the step height and the dynamics correspondently foreseen by the ANN is added to the global evolution whenever the power increases and subtracted to the total evolution whenever the power decreases. An example of an ITER-relevant wave-form is reported in Fig. 12a, in terms of the total power deposited in the entire module CS3U. During the first phase of the transient (up to t = 11 s, see inset in Fig. 12a), the power in each pancake exceeds the maximum power used in the training simulations, see also above. The power deposition in that phase has then been scaled to a mean power level over the first 90 s of transients, which guarantees the conservation of the deposited energy up to that time and, at the same time, falls inside the training range of the ANNs, see Fig. 12a. The driver, translated in terms of sigmoid wave-forms (see inset in Fig. 12a) and fed to the ANN, results in the prediction reported in Fig. 12b-c. The average error on the power evolution is ~ 10%, with an error on the peak of ~ 3%. The gain in CPU time is again ~ $10^4$.

### 4.3. Sigmoid wave-form scenario for the entire CS coil

Following the bottom-up approach allowed by the superposition of effects already verified, we can now predict the evolution of the power released to the HX of the whole CS coil when a sigmoid function such that in Fig. 6a is applied to all the different CS modules. The predictive results are reported in Fig. 13 and compared with the corresponding results computed with the 4C code, according to the Model 1 described above. The accuracy in the evolution of the thermal-hydraulic variables is excellent, and the prediction of the power evolution is on average only ~ 3.2% in relative terms far from that computed with 4C, with a gain in CPU time of the ANNs again larger than $10^4$.

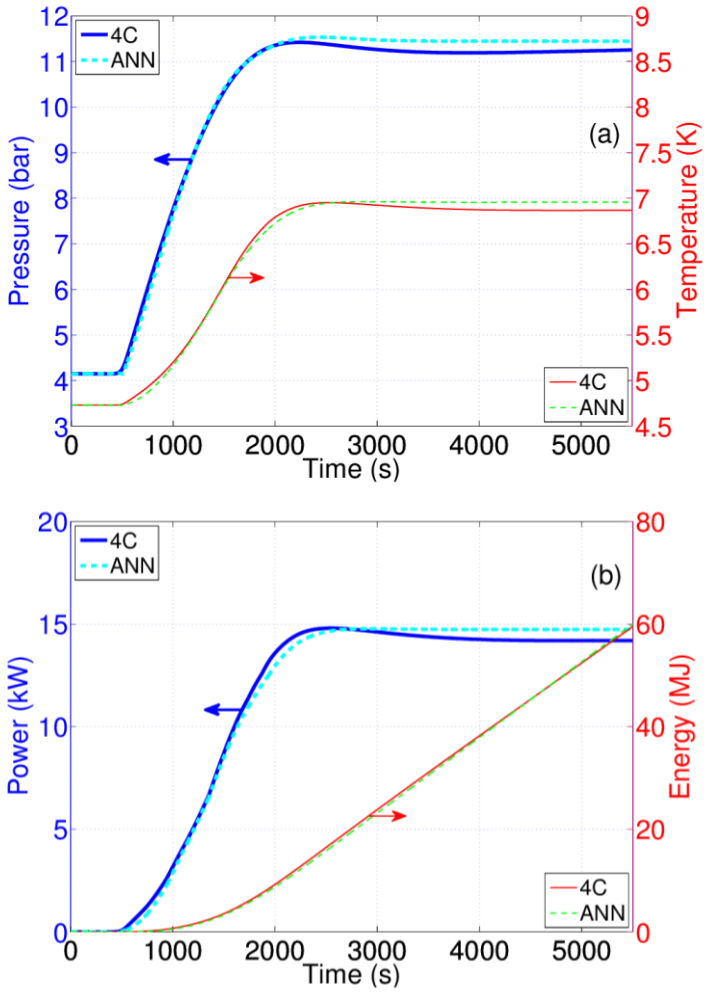


**Fig. 13 − Predictive test of ANN for the CS coil during a sigmoid evolution of the input power: (a) evolution of the pressure (left axis, thick lines) and temperature (right axis) predicted by the ANN (dashed lines) compared to the results computed by 4C (solid lines); (b) evolution of the power (left axis) and cumulative energy (right axis) released to the HX predicted by the ANN (dashed lines) and computed by the 4C code (solid lines).**

### 4.4. Plasma operation scenario for the entire CS coil

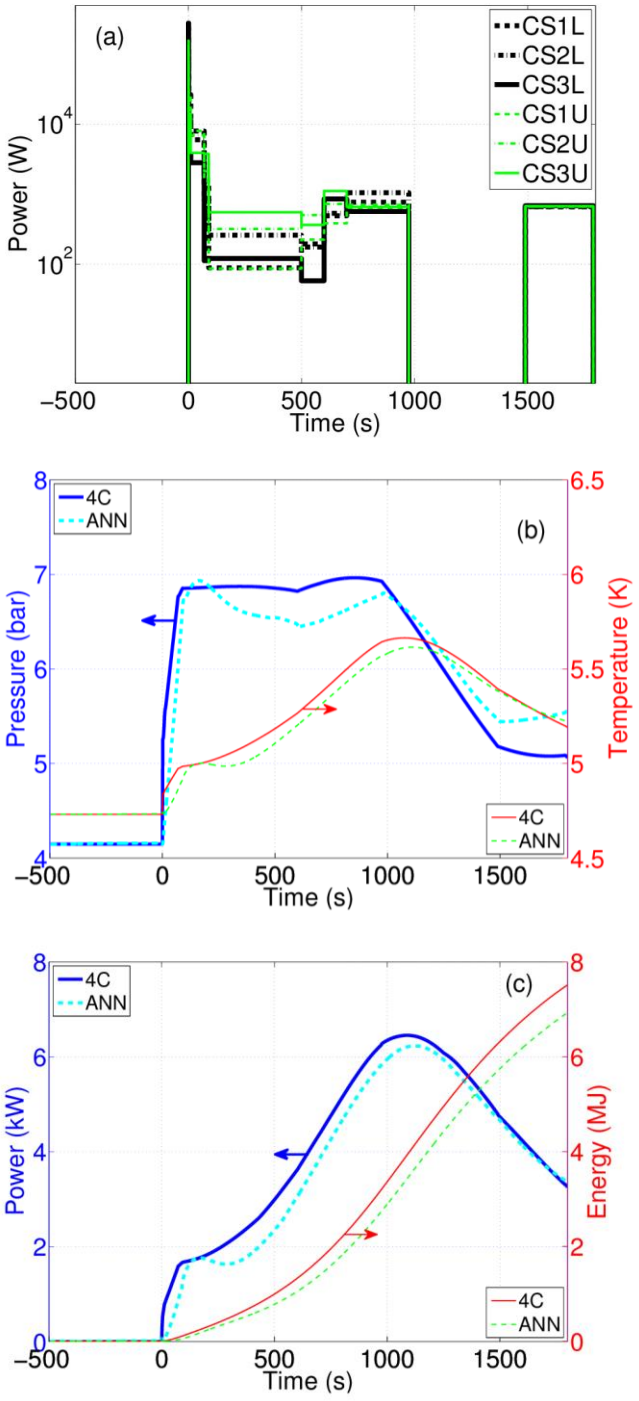


**Fig. 14 − Predictive test of ANN for the CS coil during the 15 MA standard plasma operating scenario: (a) Evolution of the heat load (AC losses) in each module, during the 15 MA standard plasma operating scenario. The pulse starts at *t* = 500 s. (b) Evolution of the pressure (left axis) and temperature (right axis) predicted by the ANN (dashed lines) compared to the results computed by 4C (solid lines). (c) Evolution of the power (left axis) and cumulative energy (right axis) released to the HX predicted by the ANN (dashed lines) and computed by the 4C code (solid lines).**

The prediction of the dynamics at the HX during a 15 MA plasma operating scenario for the whole CS coil is presented at this stage. The evolution of the heat load in each CS module is reported in Fig. 14a. For each module, the procedure described above has been applied, and the outcomes of each single ANN in terms of *p*, *T* and *dm/dt* evolution are then combined together, see Fig. 7. The overall predicted evolution of pressure and temperature at the CS HX inlet is reported in Fig. 14b, together with the corresponding computed results obtained using the 4C code. In Fig. 14c the evolution of the predicted and computed power and cumulative energy released to the LHe bath is reported. The loss of accuracy of the ANN prediction is moderate: the average error on the power evolution is ~ 8 % (computed after the SOB, see Fig. 4) and ~3.8% at the peak. The gain in CPU time with respect to the 4C simulation is ~ $5\times10^3$.

In order to check how much the good quality of the prediction relies on the representativeness of the power distribution inside each module, chosen for the ANN training, we apply the ANN developed for each module to the waveforms of all the others. Since the spatial distribution of the power in each module is different from the others, this exercise is aimed at assessing qualitatively the predictive capability of the networks when the spatial power distribution in the module is different from what has been used in the training. The results are summarized in Fig. 15, were the average error of the ANN of any CS module, evaluated when used to predict the power evolution at the HX of any of the other modules, is reported.

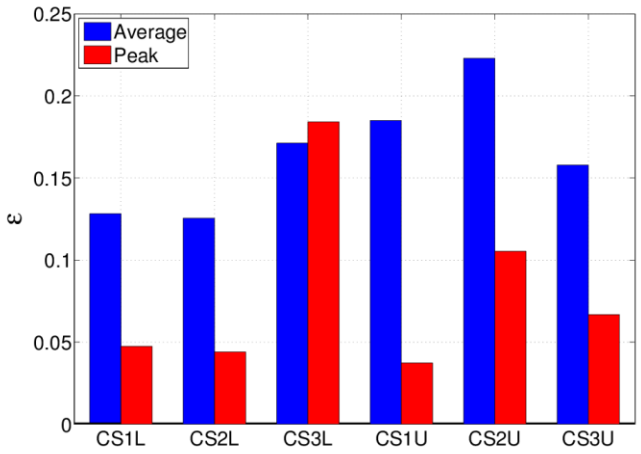


**Fig. 15 − Average error in the prediction of the power evolution when the ANN developed for a specific module is applied to the others. The average error at the peak of the power evolution is also reported.**

On average, the power evolution of any CS module can be predicted with an accuracy better than 20% by any of the other ANNs; if we look at the power peak, the accuracy in the prediction of their values is on average better than 10%. These numbers can be interpreted also as an indication of the confidence of the ANN predictions, when the ANN is applied to a scenario with different spatial power deposition with respect to the training scenarios.

## 5. CONCLUSIONS AND PERSPECTIVE

The recently proposed and validated ANN approach for the simplified dynamic modeling of the pulsed heat load from the tokamak magnets to the LHe bath has been successfully applied to the ITER Central Solenoid.

Suitable ANNs have been developed for each CS module, relying on the superposition of effects, and they have been trained using the results obtained from the 4C code, which is the state-of-the-art code for the simulation of thermal-hydraulic transients in SC magnets. The resulting ANNs have then been combined in a single network and successfully applied to the prediction of the heat load to the LHe bath in an ITER-relevant scenario: the error between ANN prediction and the reference 4C simulation is within few percent, but with a gain of orders of magnitudes in the CPU time. An assessment of the quality of the network prediction when the heating scenario hides a power distribution different from what has been used in the training has also been performed, showing that the power peak can always be computed with a relative error on average lower than 10%, if compared to the 4C results. The very good quality of the prediction shown in the paper confirms the suitability of this innovative approach for the accurate and fast evaluation of the heat load from the ITER CS coil to its LHe bath.

In perspective, the predictions of the ANNs developed here can be benchmarked against the 4C results when new heating scenarios will become available. An ANN targeted at predicting just the thermal-hydraulic response of the coil, and not focused on the HX, will also be developed and coupled to the model of the CS cryogenic circuit, to assess the capability of our simplified model to accurately cope with the control of the coil cooling loop.

## ACKNOWLEDGMENTS

The work at Politecnico di Torino has been carried out under ITER IO contract ITER/CT/12/430-554. *The views and opinions expressed herein do not necessarily reflect those of the ITER Organization.*

## REFERENCES

[1] Mitchell N, Devred A, Libeyre P, Lim B, and Savary F. The ITER magnets: design and construction status. IEEE Trans. Appl. Supercond. 2012; 22: 4200809.

[2] R.Maekawa, Process Analyses of ITER Toroidal Field Structure Cooling Scheme, presented at the CHATS-AS 2013 workshop, Boston (MA) October 9-11, 2013.

[3] Hoa C, Bon-Mardion M, Bonnay P, Charvin P, Cheynel J-N, Girard A, Lagier B, Michel F, Monteiro L, Poncet J-M, Roussel P, Rousset B, Vallcorba-Carbonell R. HELIOS helium loop for high loads smoothing: a cryogenic scaled down experiment of the cooling circuit of JT-60SA superconducting magnets. Proceedings of the 23rd International Cryogenic Engineering Conference (ICEC23) 2010; 791-6.

[4] Vallcorba R, Rousset B, Poncet J M, Chang H S, Forgeas A, Maekawa R, Serio L, Bonnay P, Bon Mardion M, Girard A, Hoa C, Lagier B, Michel F, Roussel P. ITER Cryogenics system validation tests at HELIOS test facility. Adv. Cryo. Eng. 2012; 57B: 1415-24.

[5] Bessette D, Shatil N, Zapretilina E. Simulations of the ITER Toroidal Field Coil operation with the VINCENTA code. IEEE Trans. Appl. Supercond. 2006; 16: 795-8.

[6] Maekawa R, Oba K, Takami S, Iwamoto A, Chang H S, Forgeas A, Serio L, Vallocorba R, Rousset B, Hoa C, Monteiro L. Dynamic simulation of sub-scale ITER CS/STR Cooling loop. IEEE Trans. Appl. Supercond. 2012; 22: 4704004.

[7] Zanino R, Bonifetto R, Hoa C, Savoldi Richard L. 4C modeling of pulsed-load smoothing in the HELIOS facility using a controlled by-pass valve. Cryogenics. 2013; 57: 31-44.

[8] Zanino R, Bonifetto R, Casella F, Savoldi Richard L. Validation of the 4C code against data from the HELIOS loop at CEA Grenoble. Cryogenics. 2013; 53: 25-30.

[9] Zanino R, Bonifetto R, Hoa C, Savoldi Richard L. Verification of the Predictive Capabilities of the 4C Code Cryogenic Circuit Model. To appear in Adv. Cryo. Eng. 2014.

[10] Savoldi Richard L, Casella F, Fiori B, Zanino R. The 4C code for the cryogenic circuit conductor and coil modeling in ITER. Cryogenics 2010; 50: 167-76.

[11] Savoldi Richard L, Bessette D, Bonifetto R, Zanino R. Parametric Analysis of the ITER TF Fast Discharge using the 4C code. IEEE Trans. Appl. Supercond. 2012; 22: 4704104.

[12] Savoldi Richard L, Bonifetto R, Foussat A, Mitchell N, Seo K, Zanino R. Mitigation of the Temperature Margin Reduction due to the Nuclear Radiation on the ITER TF Coils. IEEE Trans. Appl. Supercond. 2013; 23: 4201305.

[13] Fulci H, Luongo C. Development of an efficient thermo-hydraulic modeling tool to assess dynamic response of a large-scale magnet systems. Presented at the CEC/ICMC 2013 conference, Anchorage (AK), June 17-21, 2013.

[14] Savoldi Richard L, Bonifetto R, Carli S, Grand Blanc M, Zanino R. Modeling of pulsed heat load in a cryogenic SHe loop using Artificial Neural Networks. Cryogenics 2013; 57: 173-180.

[15] Miller W T, Sutton R S, Werbos P J. Neural Networks for Control. Cambridge (MA): MIT press (1990).

[16] Masini R, Padovani E, Ricotti M E, Zio E. Dynamic simulation of a steam generator by neural networks, Nuc. Eng. Des. 1999; 187: 197-213.

[17] ITER IDM. CS_conductor_and_joint_Loss_Data (35TCQT v1.0). 2009.

[18] http://www.mathworks.it/products/neural-network/ (accessed June 2, 2013).